Computer simulations of the elastic properties of liquid crystals

Douglas J. Cleaver and Michael P. Allen*
H. H. Wills Physics Laboratory, Royal Fort, Tyndall Avenue, Bristol BS8 1TL, United Kingdom
(Received 2 July 1990)

We have carried out extensive computer simulations of the Lebwohl-Lasher model of a nematic liquid crystal to determine the Frank elastic constant K for this system as a function of temperature. We use equilibrium, k-dependent, fluctuation expressions, valid at small wave vector k, and also measure the response to applied, spatially varying fields that couple to the k-dependent molecular orientation tensor. We find good agreement between these two methods. The ratio $K/\overline{P}_2^2$, where $\overline{P}_2$ is the nematic order parameter, adopts its molecular-field value at low temperatures, but rises by over 20% on approaching the nematic-isotropic transition temperature $T_{N\text{-}I}$. We note that this temperature dependence cannot be accounted for by molecular-field arguments. However, spin-wave theory correctly relates the k-dependent elastic constant with the order parameter at low temperatures, and is quite accurate up to $T/T_{N\text{-}I} \approx 0.8$. Finally, direct simulations of the Fréedericksz transition give results in reasonable agreement with the value of K as calculated by the other methods; however, we find that this is not a very efficient route to K.

I. INTRODUCTION

In a nematic liquid crystal, the distribution of molecular positions is translationally invariant but the orientational distribution shows preferential alignment along some axis. This axis is called the director. The degree of alignment in a macroscopic region containing N molecules is conveniently measured using the second-rank order parameter $\overline{P}_2$, given by

$$\overline{P}_2 = \langle P_2(\cos\theta_i)\rangle_0 = \left\langle \frac{1}{N}\sum_{i=1}^{N} \tfrac{3}{2}\{[\mathbf{n}(\mathbf{r}_i)\cdot\mathbf{e}_i]^2 - \tfrac{1}{3}\} \right\rangle_0 . \tag{1}$$

The angle brackets $\langle\rangle_0$ and the overbar both indicate equilibrium ensemble averages in the absence of an external field. $\mathbf{n}(\mathbf{r}_i)$ and $\mathbf{e}_i$ are unit vectors along the local director and the axis of molecule i, respectively, and θ_i is the angle between them. P_2 is the second Legendre polynomial. The director may be taken to be a slowly changing function of $\mathbf{r}$. Indeed, microscopically (in the absence of a defect or an externally induced distortion) it can be taken to be constant, the $\mathbf{e}_i$ being distributed about it according to some distribution function $\mathcal{P}(\mathbf{n}\cdot\mathbf{e}_i)$; $\overline{P}_2$ is the lowest-order nonvanishing average over this distribution.

At long range, orientational correlations decay slowly (algebraically) with distance. Short-wavelength fluctuations are unimportant and become ill-defined here because of the spatial coarse-graining implicitly needed to define $\mathbf{n}(\mathbf{r})$. Those on macroscopic length scales, λ, are more important, however: due to the broken symmetry associated with the director[1,2] they can be long-lived, decaying with typical hydrodynamic time scales $\propto \lambda^2$.

For nematic phase stability, any inhomogeneity in the director field must lead to a free energy increase, $\Delta\mathcal{F}$. Since (as shown by Frank[3]) all such distortions can be reduced to a combination of splay, twist, and bend deformations, this can be expressed phenomenologically as

$$\Delta\mathcal{F} = \tfrac{1}{2}\int d\mathbf{r}\{\, K_1[\nabla\cdot\mathbf{n}(\mathbf{r})]^2 + K_2\{\mathbf{n}(\mathbf{r})\cdot[\nabla\times\mathbf{n}(\mathbf{r})]\}^2 + K_3\{\mathbf{n}(\mathbf{r})\times[\nabla\times\mathbf{n}(\mathbf{r})]\}^2 . \tag{2}$$

The parameters K_1, K_2, and K_3 in Eq. (2) are the splay, twist, and bend Frank elastic constants respectively.

The Frank constants play a role in a great number of the properties characteristic of nematic liquid crystals. As well as determining the relaxation of director field inhomogeneities, K_1, K_2, and K_3 govern the shapes of defects (disclinations) (Ref. 3) and flow patterns,[4] the extent to which liquid crystals transmit torques and their response to applied fields.[1,5] Since the last two of these are the main properties exploited in liquid-crystal displays and switching devices, developments regarding the values and variation of the elastic constants clearly have technological relevance. At a more fundamental level, the behavior of the Frank constants at the nematic-isotropic (N-I) transition is still unclear and warrants further study.

Traditionally, experimental determinations of the Frank constants have been based on the observation of the Fréedericksz transition.[6] In this a sample of liquid crystal in slab geometry, subject to two aligning fields (one due to surface coupling, the other to an externally applied bulk field, H), shows a second-order bulk orientation transition at a critical field, H_c. Saupe[7] derived a continuum theory for the Fréedericksz transition and showed that both the value of H_c and the behavior of the

slab for $H > H_c$ are determined by the Frank constants. Subsequently, K_1, K_2, and K_3 have been found experimentally through the measurement of various optical[8–10] and other[10,11] properties of such samples.

A different technique used to determine the Frank constants is that based on quasielastic Rayleigh scattering. Through the application of fluctuation-quenching fields, this method has been used to give results with accuracies approaching those obtained using well-developed Fréedericksz systems.[12] Another recent development has seen accurate estimation of the twist constant K_2 (which, for geometrical reasons, has been the hardest of the three to measure using the older techniques) by direct torque measurements.[13]

The Frank constants have also been investigated by computer simulation and theory. Three types of model have been used: lattice models, hard-particle models, and soft-particle models.

In the Lebwohl-Lasher model,[14] which has its origins in the work of Maier and Saupe,[15] a system of spins on a simple cubic lattice with nearest-neighbor interactions is considered. This model, though idealized, has proved a valuable test bed for theory and simulation, and it is the main subject of this paper. Extensive studies of its bulk[16–18] and surface[19–21] behavior have shown it to exhibit many of the properties characteristic of the N-I transition (e.g., a small latent heat and pretransitional divergence of orientational correlations). The simplicity of the model is a major advantage in simulations since it enables systems of tens of thousands of molecules to be studied.

For this particular model all of the Frank constants are equivalent, $K_1, K_2, K_3 = K$. Priest[22] calculated K within a simple molecular-field approximation and Simpson[23] made the first attempt to measure it through a computer simulation of the Fréedericksz transition. We return to this, and give full details of the model, in the following sections.

Many theoretical predictions regarding K_1, K_2, and K_3, inspired by the work of Onsager,[24] are based on systems of hard rods, spherocylinders, or ellipsoids.[25,26] There has been one attempt, by Allen and Frenkel,[27] to calculate the Frank constants for hard ellipsoids and spherocylinders by computer simulation. A limitation of this work, however, was the small system size that had to be employed (a few hundred molecules at most). Although dependence of K_1, K_2, and K_3 on system size seems not to be very serious,[28] there remains considerable uncertainty in the results given in Ref. 27 since the method used therein involves an extrapolation to low wave vector. In the current work we are able to examine much larger system sizes, and hence go to much lower wave vector. This enables us to make a check on the method employed for the smaller hard-body systems by Allen and Frenkel. Finally, some attempts have been made to calculate K_1, K_2, and K_3 for soft-potential models[29,30] but to our knowledge no comparisons with simulation have been made as yet.

The main body of the work presented here consists of two different Monte Carlo measurements of the Frank constant of the Lebwohl-Lasher lattice model. The first method used is the same as that employed in Ref. 27. The second, based on the system's response to a spatially dependent field, is a new approach to this problem. Through the use of linear-response theory, however, the two can be shown to be formally equivalent. In addition to these two techniques, we also describe the results of a simulation of the Fréedericksz transition. Here we follow Ref. 23, but extend the work to much larger system sizes and simulation run lengths.

In Sec. II, we give the theoretical bases for these techniques. Section III contains the simulation details and results. Finally, we compare the different sets of simulation results with each other and with theoretical predictions, and draw our conclusions.

II. THEORY

In the Lebwohl-Lasher model[14] the molecular centers of mass are held fixed at the sites of a simple cubic lattice. The molecules are treated as ("headless") vectors and are free to rotate about their centers subject to the nearest-neighbor interaction

$$\mathcal{H}_0 = -\varepsilon \sum_{<i,j>} P_2(\cos\theta_{i,j}) = -\varepsilon \sum_{<i,j>} P_2(\mathbf{e}_i \cdot \mathbf{e}_j), \qquad (3)$$

where θ_{ij} is the angle between the axes of neighboring molecules i and j. The lattice spacing a and thus the number density N/V are set to unity. The (positive) coupling constant ε is also set to 1 and we measure temperature in reduced units, $T^* = k_B T/\varepsilon$. The bulk transition temperature in the thermodynamic limit is estimated[18] to be $T^*_{N\text{-}I} = 1.1255$. Equation (3) is degenerate to uniform rotations of all molecules, and this leads to the equivalence $K_1, K_2, K_3 = K$ mentioned previously. We define a dimensionless elastic constant $K^* = Ka/\varepsilon$.

In the following we use both a coordinate system (x, y, z) based on the cubic lattice and a system $(1, 2, 3)$ based on the director $\mathbf{n}$, which is taken to lie in the 3 direction. For the unperturbed Hamiltonian of Eq. (3) the angular and spatial coordinates are separate, and it is not necessary to relate these two coordinate systems. When we model the effect of an applied field it becomes necessary to specify the transformation $(x, y, z) \leftrightarrow (1, 2, 3)$.

Spatial variations of molecular orientation may be described by the wave-vector-dependent ordering tensor $\hat{\mathbf{Q}}(\mathbf{k})$ whose Cartesian components are given by

$$\hat{Q}_{\alpha\beta}(\mathbf{k}) = \frac{V}{N} \sum_{i=1}^{N} \tfrac{3}{2}(e_{i\alpha}e_{i\beta} - \tfrac{1}{3}\delta_{\alpha\beta}) \exp(i\mathbf{k} \cdot \mathbf{r}_i),$$

$$\alpha, \beta = x, y, z \qquad (4)$$

where $\delta_{\alpha\beta}$ is the Kronecker delta. The spatial Fourier transform of this is the orientation density

$$Q_{\alpha\beta}(\mathbf{r}) \equiv \frac{1}{V}\sum_{\mathbf{k}} \hat{Q}_{\alpha\beta}(\mathbf{k}) \exp(-i\mathbf{k}\cdot\mathbf{r}). \quad (5)$$

In the unperturbed system the average orientation density is a constant, $\langle \mathbf{Q}(\mathbf{r})\rangle_0 = \langle \hat{\mathbf{Q}}(\mathbf{0})\rangle_0/V$. The bulk order parameter $\overline{P}_2$ is given by the highest eigenvalue of $\langle \mathbf{Q}\rangle_0$, and $\mathbf{n}$ is the corresponding eigenvector;[16,31] this prescription is equivalent to Eq. (1), once the director has been determined. In the director-based coordinate system with $\mathbf{n} = (0,0,1)$, $\langle \mathbf{Q}\rangle_0$ is diagonal with $\langle Q_{11}\rangle_0 = \langle Q_{22}\rangle_0 = -\frac{1}{2}\overline{P}_2$ and $\langle Q_{33}\rangle_0 = \overline{P}_2$.

To describe orientational fluctuations we follow Forster.[2] Without loss of generality we consider a wave vector in the 1-3 plane of the director-based system, $\mathbf{k} = (k_1, 0, k_3)$. Then, a transformation of Eq. (2) into reciprocal space gives a free-energy quadratic in the Fourier components, $\hat{n}_1(\mathbf{k})$, $\hat{n}_2(\mathbf{k})$, of the director fluctuations. From equipartition, this yields the thermal average[2]

$$\left\langle \hat{Q}_{\alpha 3}(\mathbf{k})\hat{Q}_{\alpha 3}(-\mathbf{k})\right\rangle_0 = \frac{9}{4}\left(\frac{\overline{P}_2^2 V k_B T}{K_\alpha k_1^2 + K_3 k_3^2}\right), \quad \alpha = 1,2 \quad (6)$$

valid in the limit of small $k = |\mathbf{k}|$. Allen and Frenkel[27] used this expression to calculate K_1, K_2, and K_3 for hard ellipsoids and spherocylinders, through double polynomial fits in the variables k_1^2 and k_3^2 to the inverse of $\langle \hat{Q}_{\alpha 3}(\mathbf{k})\hat{Q}_{\alpha 3}(-\mathbf{k})\rangle_0$. As well as the need to measure these fluctuation values to a sufficient statistical precision, this method requires that a large number of k values be studied, particularly at low k. These can all be accumulated in a single simulation, but clearly the system size imposes a lower limit on k.

Linear-response theory provides an alternative way of measuring the K_1, K_2, and K_3. Consider a perturbed Hamiltonian of the form

$$\mathcal{H} = \mathcal{H}_0 - \Delta\mathcal{H}, \quad (7)$$

where $\mathcal{H}_0$ is the unperturbed Hamiltonian. Averages measured in the perturbed system $\langle\rangle$ are related to equilibrium ensemble averages as follows:

$$\langle A\rangle = \frac{1}{k_B T}\langle A\Delta\mathcal{H}\rangle_0. \quad (8)$$

Formally the choice $\Delta\mathcal{H} = F\hat{Q}_{\alpha 3}(\mathbf{k})$, where F is the strength of a field coupling to an element of the ordering matrix and $\mathbf{k}$ a chosen wave vector, would lead to a measurement of the fluctuation average of Eq. (6) via the response

$$\langle \hat{Q}_{\alpha 3}(-\mathbf{k})\rangle = \frac{F}{k_B T}\langle \hat{Q}_{\alpha 3}(\mathbf{k})\hat{Q}_{\alpha 3}(-\mathbf{k})\rangle_0. \quad (9)$$

In practice, a real-valued perturbation is applied, typically of the form

$$\Delta\mathcal{H} = F\ \mathrm{Re}\ \hat{Q}_{\alpha 3}(\mathbf{k}) = F\tfrac{1}{2}[\hat{Q}_{\alpha 3}(\mathbf{k}) + \hat{Q}_{\alpha 3}(-\mathbf{k})] = F\left(\frac{V}{N}\sum_{i=1}^{N}\tfrac{3}{2}e_{i\alpha}e_{i3}\cos(\mathbf{k}\cdot\mathbf{r}_i)\right), \quad \alpha = 1,2 \quad (10)$$

and this gives the responses

$$\langle \hat{Q}_{\alpha 3}(\mathbf{k})\rangle = \langle \hat{Q}_{\alpha 3}(-\mathbf{k})\rangle = \frac{F}{2k_B T}\langle \hat{Q}_{\alpha 3}(\mathbf{k})\hat{Q}_{\alpha 3}(-\mathbf{k})\rangle_0 \quad (11)$$

with $\langle \hat{Q}_{\alpha 3}(\mathbf{k}')\rangle = 0$ for $\mathbf{k}' \neq \mathbf{k}$. In terms of the real-space orientation density $Q_{\alpha\beta}(\mathbf{r})$ this corresponds to an oscillatory profile

$$\langle Q_{\alpha 3}(\mathbf{r})\rangle = \frac{\langle \hat{Q}_{\alpha 3}(\mathbf{k})\hat{Q}_{\alpha 3}(-\mathbf{k})\rangle_0}{V k_B T} F\cos(\mathbf{k}\cdot\mathbf{r}) = \frac{9}{4}\left(\frac{\overline{P}_2^2}{K_\alpha k_1^2 + K_3 k_3^2}\right) F\cos(\mathbf{k}\cdot\mathbf{r}), \quad \alpha = 1,2 \quad (12)$$

where we have again made the choice $\mathbf{k} = (k_1, 0, k_3)$. Thus, by measuring the amplitude of the response to a chosen perturbation we can evaluate K_1, K_2, and K_3. In practice, a space-fixed perturbation would be applied, and it would be necessary to fix the director coordinate system with respect to the lattice.

In simulation terms, the advantage of this approach is that $\langle \hat{Q}_{\alpha\beta}(\mathbf{k})\rangle$ is measurable with greater statistical precision (signal-to-noise ratio) than $\langle \hat{Q}_{\alpha\beta}(\mathbf{k})\hat{Q}_{\alpha\beta}(-\mathbf{k})\rangle_0$, if F is made sufficiently large. This is subject to the condition that the applied field is small enough to ensure the applicability of linear-response theory. An additional drawback is that each simulation produces results for one $\mathbf{k}$ vector only: thus it is not immediately obvious whether the applied-field method is more or less efficient than the equilibrium fluctuation method. Note that the requirement to extrapolate to low k, and hence the need for large system sizes, is unaltered.

The third technique used in this paper is a direct simulation of the Fréedericksz transition. Saupe's[7] formulation of this problem is well documented in the standard texts[1,5] and so we limit ourselves to a brief description here before quoting the final equations.

It is well established that the director of a nematic liquid crystal in contact with a specially treated glass plate can be anchored rigidly along some easy axis. Thus, a sample of liquid crystal confined between a parallel arrangement of two such plates of common easy axis can be considered as a slab of nematic liquid crystal with known director and two pinned boundaries. Saupe's theory applies to the cases in which this director is either parallel to or perpendicular to the plates. In such cases, a magnetic field of magnitude H applied perpendicular to the initial director is shown to reorient that director if

$$H > H_{c,\alpha} = \frac{\pi}{L}\left(\frac{K_\alpha}{\chi_a}\right)^{1/2}, \quad \alpha = 1,2,3 \tag{13}$$

where L is the slab thickness and χ_a is the volume anisotropy in the diamagnetic susceptibility. The choice of α in Eq. (13) is determined by the relative orientations of the plates, field, and easy axis. The theory also predicts the size of the deformation at the center of such a cell for $H > H_{c,\alpha}$. In its general form this expression involves a ratio of two Frank constants, but for the case where $K_{1-3} = K$ it reduces to

$$\frac{H}{H_c} = \frac{2}{\pi}\int_0^{\pi/2} d\lambda \frac{1}{(1-\sin^2\theta^{\rm mid}\sin^2\lambda)^{1/2}}, \tag{14}$$

where $\theta^{\rm mid}$ is the angular deformation at the midpoint of the sample and $\sin\lambda = \sin\theta/\sin\theta^{\rm mid}$. Saupe's expressions are well obeyed in experimental studies of these systems.[8–11] Furthermore, it is found that for some property A, the results from different cell sizes are successfully mapped onto each other by the scaling form $A = A(HL)$ for all but the smallest L . This breakdown at small L is usually attributed to the increased relative effect of imperfect surface anchoring as the cell thickness is decreased.

A simulation of this slab geometry is easily set up with periodic boundary conditions applied only in the x and y directions. Surface ordering is then achieved through the use of sheets of perfectly aligned molecules positioned at the top and bottom surfaces. We choose to align these surface molecules in the y direction. A perturbation term in the Hamiltonian of Eq. (7), taking the form

$$\Delta\mathcal{H} = F\hat{Q}_{xx}(\mathbf{0}) = F\frac{V}{N}\sum_i P_2(e_{ix}) \tag{15}$$

represents the effect of a bulk field, of strength F, coupling to the component e_{ix} of each molecular axis vector, and favoring alignment in the x direction. For this Hamiltonian an essentially equivalent analysis to that of Saupe can be carried out: this is described in Appendix A. The critical field is given by

$$F_c = \frac{K\pi^2}{3L^2\overline{P}_2}, \tag{16}$$

where L is the slab thickness. The appropriate scaling form is $A = A(FL^2)$ rather than $A = A(HL)$. The deformation at the center of the slab is linked to the applied field, for $F > F_c$, by

$$\frac{F}{F_c} = \left(\frac{2}{\pi}\int_0^{\pi/2} d\lambda \frac{1}{(1-\sin^2\theta^{\rm mid}\sin^2\lambda)^{1/2}}\right)^2 \tag{17}$$

and $\sin^2\theta^{\rm mid} = (n_x^{\rm mid})^2$, the square of the appropriate component of the director.

III. SIMULATION DETAILS AND RESULTS

All of the simulations for this work were carried out using standard Metropolis Monte Carlo algorithms on a DAP 510-8 computer, a massively parallel computer which is ideally suited to lattice systems of this kind. Full technical details are given elsewhere.[20]

A. Unperturbed system

Simulations of the unperturbed Lebwohl-Lasher model were carried out using a system with periodic boundary conditions in all three directions. All measurements were averaged over blocks of 1024 cycles, where one cycle corresponds to one attempted move per molecule. Error estimates were made on the assumption that results from different blocks were uncorrelated.

Extensive simulations were carried out at five temperatures, $T^* = 0.40$, 0.75, 0.90, 1.00, and 1.08, and shorter runs were conducted at $T^* = 0.10$, 0.20, and 0.30. In all these cases a 32 768-particle system ($32 \times 32 \times 32$) was employed. To test for size dependence, the run at $T^* = 0.75$ was repeated with a system of 16 384 spins, being half as wide in the z direction. Full details can be found in Table I. Wherever possible equilibration runs were started from the final configurations obtained at neighboring temperatures.

TABLE I. Fluctuation measurement results. Estimated errors in the final digit are given in parentheses.

T^*	Run length[a]	$\overline{P}_2$	$\overline{P}_4$	$K^*/\overline{P}_2^2$
0.10	14 [6]	0.9749(1)	0.9189(2)	3.026(7)
0.20	14 [6]	0.9488(1)	0.8393(3)	
0.30	14 [6]	0.9213(1)	0.7611(3)	
0.40	48 [12]	0.8922(1)	0.6845(3)	3.177(3)
0.75	48 [12]	0.7672(2)	0.4216(5)	3.355(3)
0.75[b]	48 [12]	0.7668(2)		3.377(6)
0.90	48 [12]	0.6863(4)	0.3014(5)	3.492(5)
1.00	48 [12]	0.6038(4)	0.2162(5)	3.594(5)
1.08	48 [12]	0.4822(6)	0.1256(5)	3.693(6)

[a]Run lengths are measured in "blocks" of 1024 attempted moves per spin. The figures quoted are the production run length and (in square brackets) the equilibration run length.
[b]Results for the $32 \times 32 \times 16$ system; all others are for $32 \times 32 \times 32$.

The order parameter $\overline{P}_2$ was calculated at each temperature from the largest eigenvalue of the run-averaged ordering matrix. $\overline{P}_4$ was calculated using the method described by Fabbri and Zannoni.[18] Director fluctuations were measured as follows. After each cycle, all of the molecules in the system were rotated equally such that the mean director (defining the 3 direction) was aligned with the z axis. (The Hamiltonian is invariant to this rotation.) The 1 and 2 directions were taken to lie along the x and y axes. In this way variation of the components k_1, k_3 of the wave vectors, due to director drift in the space-fixed axis system, was avoided. Two three-dimensional Fourier transforms were then performed to obtain values for the two independent functions $\langle \hat{Q}_{\alpha 3}(\mathbf{k})\hat{Q}_{\alpha 3}(-\mathbf{k})\rangle_0$, $\alpha = 1, 2$. Since these modes are equivalent, the two sets of results were simply averaged before fitting.

Low-k fits of the orientational fluctuations to the form

$$\langle \hat{Q}_{\alpha 3}(\mathbf{k})\hat{Q}_{\alpha 3}(-\mathbf{k})\rangle_0^{-1} \approx c_2 k^2 + c_4 k^4 \tag{18}$$

are shown in Fig. 1. In each case we used all reciprocal-lattice points for which $k^2 \leq 30k_{\min}^2$ where $k_{\min} = 2\pi/32$. The fits are excellent, with very little curvature: the coefficients c_4 are very small throughout. This confirms that the range of k available in our simulations was sufficient for Eq. (6) to hold.

The coefficients c_2 from these fits yield values for $K^*/\overline{P}_2^2$. These are presented in Table I. $\overline{P}_2$, K^*, and $K^*/\overline{P}_2^2$ are plotted as functions of temperature in Fig. 2. These are the principal results of this paper. We note that the ratio $K^*/\overline{P}_2^2$ increases as the transition temperature is approached from below. A detailed comparison with theoretical predictions follows in Sec. IV.

We note that a slightly larger value of $K^*/\overline{P}_2^2$ is seen for the 16 384-spin system than for the 32 768-spin system at the same temperature, while the order parameter $\overline{P}_2$ is essentially unaltered. This is consistent with the "stiffening" expected to result from a decrease in the distance between the periodic images of a given spin. The measured shift is very small, however, indicating little effect of system size on these simulations.

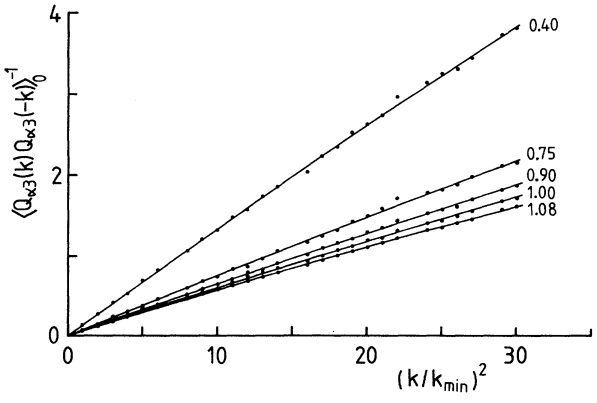

FIG. 1. $\langle Q_{\alpha 3}(\mathbf{k})Q_{\alpha 3}(-\mathbf{k})\rangle_0^{-1}$ plotted vs $(k/k_{\min})^2$ where $k_{\min} = 2\pi/32$, at temperatures $T^* = 0.40$, 0.75, 0.90, 1.00, and 1.08. In each case the statistical errors are smaller than the plotting symbol. The curves are fits obtained using Eq. (18).

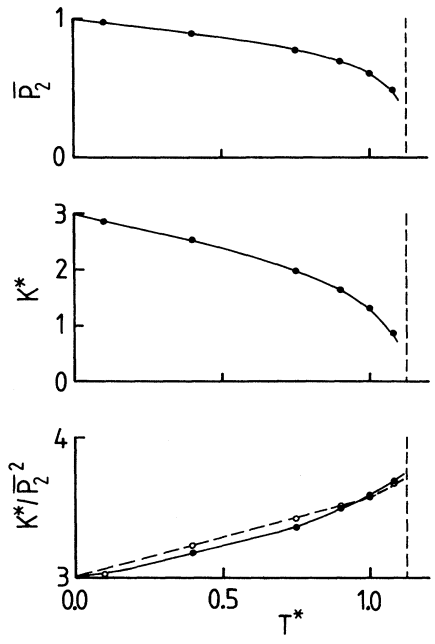

FIG. 2. Temperature variation of K^*, $\overline{P}_2$, and the ratio $K^*/\overline{P}_2^2$. The solid circles denote results from the unperturbed simulations; the open circles are based on Eq. (20) with fitted parameters c_{22}, c_{24}. The lines through the data points are to guide the eye. The vertical dashed line indicates the nematic-isotropic phase transition temperature $T^*_{N\text{-}I} = 1.1255$.

B. Perturbed system

Simulations of the perturbed system were carried out using the Hamiltonian described above but with the additional perturbation term of Eq. (10). We made the $(1, 2, 3)$ and (x, y, z) axis systems coincident, the director lying along the 3 direction as before, and chose to apply the perturbation to the $\hat{Q}_{13}$ matrix element [thus taking $\alpha = 1$ in Eq. (10)]. We took $\mathbf{k} = (0, 0, k)$, with $k/k_{\min} = 1, 2, 3$. Results were obtained for a $32 \times 32 \times 32$ system at reduced temperatures $T^* = 0.75$ and 0.9, and to test for size dependence two runs at $T^* = 0.75$ were repeated for a system half as wide in the z direction. Simulation parameters appear in Tables II and III.

As in the unperturbed case, after each cycle a uniform rotation of all molecules must be carried out to align the director with the z axis. This is necessary for the orientational perturbation to take the required form. Strictly, this rotation does not leave the perturbed Hamiltonian invariant, but for a large system size the error incurred is entirely negligible.

Simulations were carried out for a range of F at each given temperature and wave number. Starting with the

TABLE II. Perturbed system results for $T^* = 0.75$.

$32k/2\pi$	F	Run length[a]	A	$K^*/\overline{P}_2^2$
1	0.006 25	60 [18]	0.111	3.29
1[b]	0.0125	36 [12]	0.209	3.49
1[b]	0.025	36 [12]	0.351	4.16
2	0.0125	60 [24]	0.054	3.36
2	0.025	60 [18]	0.109	3.35
2[b]	0.05	36 [12]	0.205	3.56
2[c]	0.0125	60 [24]	0.054	3.37
2[c]	0.025	60 [18]	0.109	3.36
3	0.025	60 [24]	0.049	3.33
3	0.05	48 [24]	0.097	3.35

[a]Run lengths are measured in "blocks" of 1024 attempted moves per spin. The figures quoted are the production run length and (in square brackets) the equilibration run length.
[b]Outside limiting linear regime (see text).
[c]Results for the 32 × 32 × 16 system; all others are for 32 × 32 × 32.

largest F, the system was first equilibrated from a perfectly ordered configuration. Then, a number of production runs were executed, each one using the same equilibrated system as its starting point. On completion of the runs at one phase point, the value of F was halved and the process repeated, the initial equilibration starting from a configuration taken at the previous field strength.

During each run, the ordering matrices $\mathbf{Q}(\mathbf{r})$ were calculated and averaged over sheets of constant z. On completion, the function $\langle Q_{13}(z)\rangle$ was fitted to the form $A\cos kz$. From Eq. (12) we expect an amplitude

$$A = \frac{9}{4}\left(\frac{\overline{P}_2^2}{K^*k^2}\right)F. \tag{19}$$

In Fig. 3 we plot Ak^2 as a function of F for various wave numbers at $T^* = 0.75$. The results for $T^* = 0.9$ are very similar in form. At sufficiently low values of F, the results for different k become consistent with each other, and show a linear variation with F. For each run a value of $K^*/\overline{P}_2^2$ was deduced from Eq. (19). The run lengths and results for these phase points are summarized in Tables II and III.

TABLE III. Perturbed system results for $T^* = 0.90$.

$32k/2\pi$	F	Run length[a]	A	$K^*/\overline{P}_2^2$
1	0.006 25	60 [18]	0.109	3.33
1[b]	0.0125	48 [18]	0.201	3.63
1[b]	0.025	36 [12]	0.340	4.29
2	0.0125	60 [24]	0.053	3.47
2	0.025	48 [24]	0.105	3.47
2[b]	0.05	36 [12]	0.198	3.68
3	0.025	60 [24]	0.047	3.46
3	0.05	48 [24]	0.095	3.43

[a]Run lengths are measured in "blocks" of 1024 attempted moves per spin. The figures quoted are the production run length and (in square brackets) the equilibration run length.
[b]Outside limiting linear regime (see text).

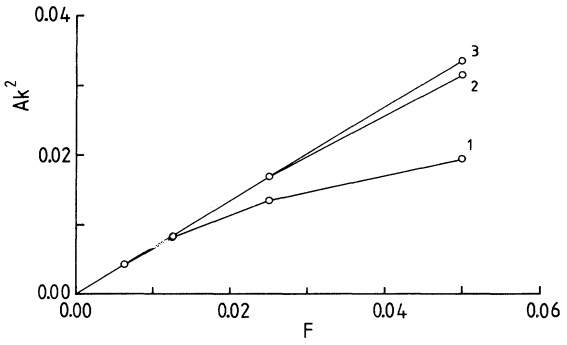

FIG. 3. Response Ak^2 vs applied field F for $T^* = 0.75$ and wave numbers $k/k_{\min} = 1, 2, 3$ ($k_{\min} = 2\pi/32$). The lines are to guide the eye.

We observed significant deviations from the asymptotic linear response for amplitudes $A > 0.12$. Five points at each temperature lie within the linear regime defined by $A < 0.12$. Given standard errors of order 1% in each of these, the spread of results is reasonable. Linear least-squares fits of the function Ak^2 versus F for these points give our final perturbed-system estimates of $K^*/\overline{P}_2^2 = 3.349$ at $T^* = 0.75$ and $K^*/\overline{P}_2^2 = 3.429$ at $T^* = 0.90$. We note that these values are in good agreement with those found using the equilibrium fluctuation expression. Although there are too few data points for any rigorous error estimation to be carried out here, the spread of the results suggests that these values have an error of less than 1% overall.

We note from Fig. 3 that the linear regime in F is least extensive for the longest-wavelength perturbations. This is as expected, since for fixed F the response amplitude is predicted to vary as k^{-2}: saturation of the response occurs more readily for the longer-wavelength perturbations.

As in the unperturbed case, we note that slightly larger values of $K^*/\overline{P}_2^2$ are seen for the 32×32×16 systems than for the 32 × 32 × 32 systems under the same conditions. Once more the measured shifts are very small.

C. Fréedericksz transition

In the simulations of the Fréedericksz transition periodic boundary conditions were applied in the x and y directions, while the top and bottom sheets of surface molecules were aligned in the y direction. The perturbation given in Eq. (15) was applied to represent the effect of a bulk field favoring alignment in the x direction. We used a 16 × 16 × 34 system (i.e., 32 mobile layers and two fixed ones) and the simulations were limited to a single temperature, $T^* = 1.0$. We found that very long runs

were required: at several values of the field close to F_c, over half a million cycles were used. This was the reason for the use of a smaller system size in these simulations, and the restriction to one value of T^*.

These extremely long run times were necessary because for $F > F_c$ two degenerate orientational states exist. At large F one or the other state is indefinitely metastable, but as $F \rightarrow F_c+$ flips between the two states become more frequent. This leads to large orientational fluctuations and poor statistics. An explicit example of this behavior is given in the "time"-series (with "time" in units of 1024 Monte Carlo cycles) in Fig. 4. We observe the orientation of the mean director $\langle \mathbf{n}^{\text{mid}} \rangle$ at the midpoint of the slab (actually averaged over the two central layers). The component $\langle n_y^{\text{mid}} \rangle$ is chosen to be positive throughout, to fix the overall sign, and our interest lies in the behavior of n_x^{mid} ($\equiv \sin\theta^{\text{mid}}$). For $F > F_c$, $\langle n_x^{\text{mid}\,2} \rangle$ is nonzero: there are two degenerate states corresponding to $n_x^{\text{mid}} > 0$ and $n_x^{\text{mid}} < 0$. In Fig. 4, the system is clearly seen to be flipping between these states. These flips are analogous to the spontaneous jumps made by an Ising system in zero field, below the phase transition, between two degenerate states with nonzero spontaneous magnetization. The transitional flips became more frequent and the change in n_x^{mid} less dramatic, as $F \rightarrow F_c+$. However, the associated slow fluctuations hinder equilibration, as mentioned previously, and necessitate rather long runs.

The simulations themselves were carried out very much as before. The first run was made with a large field strength, and lower field systems were prepared using configurations from neighboring phase points. In view of the equilibration doubts present here, however, long single runs were employed in preference to a number of short ones. The details of these simulations are given in Table IV.

TABLE IV. Fréedericksz transition results for $T^* = 1.00$. Estimated errors in the final digit are given in parentheses.

F	Run length[a]	$\langle \sin^2\theta^{\text{mid}} \rangle$	$\overline{P_2}^{\text{mid}}$
0.0	145 [25]	0.023(3)	0.621
0.004	350 [70]	0.042(3)	0.620
0.005	500 [110]	0.048(3)	0.619
0.006	430 [100]	0.066(5)	0.619
0.007	450 [150]	0.13(1)	0.619
0.008	500 [140]	0.21(1)	0.620
0.0085	450 [150]	0.23(1)	0.620
0.009	500 [90]	0.38(1)	0.621
0.0095	430 [140]	0.39(1)	0.622
0.01	450 [170]	0.40(1)	0.622
0.0105	450 [150]	0.49(1)	0.622
0.011	150 [50]	0.61(1)	0.623
0.012	105 [60]	0.66(1)	0.624
0.013	90 [30]	0.74(1)	0.625
0.015	100 [20]	0.81(1)	0.626
0.02	100 [20]	0.901(5)	0.631

[a]Run lengths are measured in "blocks" of 1024 attempted moves per spin. The figures quoted are the production run length and (in square brackets) the equilibration run length.

The signature of the transition, needed to determine F_c, is an increase in the order parameter $\langle \sin^2\theta^{\text{mid}} \rangle$ ($\equiv \langle n_x^{\text{mid}\,2} \rangle$) at the midpoint of the slab (again averaged over the two central layers). The measured F dependence of $\langle \sin^2\theta^{\text{mid}} \rangle$ is shown in Fig. 5. For $F < F_c$, the Saupe theory predicts that this quantity should be zero; in fact, it does not vanish even at $F = 0$ because of fluctuations. This is the usual behavior expected of an order parameter

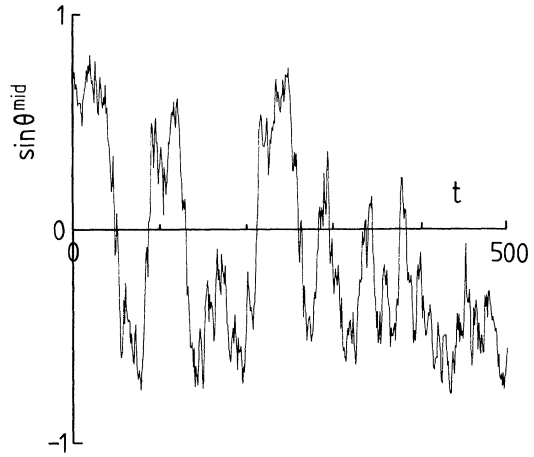

FIG. 4. Time evolution of the angular distortion $\sin\theta^{\text{mid}} = n_x^{\text{mid}}$ in the middle of the slab, with time t measured in blocks of 1024 Monte Carlo cycles. The system temperature $T^* = 1.0$, close to the Fréedericksz transition, and the applied field $F = 0.008$.

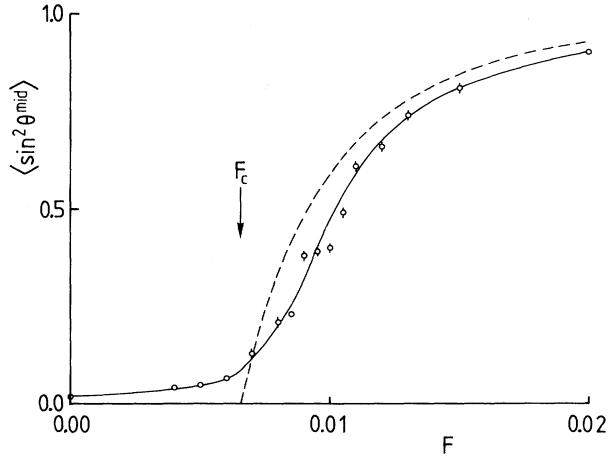

FIG. 5. Field-induced response $\langle \sin^2\theta^{\text{mid}} \rangle = \langle n_x^{\text{mid}\,2} \rangle$ at the middle of the slab vs applied field F at $T^* = 1.0$, showing the Fréedericksz transition. The solid line is to guide the eye. The arrow indicates the critical field F_c calculated from the value of K measured in the unperturbed simulation at this temperature. The dashed line is the prediction of the Saupe theory, Eq. (17).

in a finite system.

Rather than calculating K^* directly from our Fréedericksz results, we have determined the critical field strength predicted by Eq. (16), assuming $\overline{P}_2(z) \simeq$ const, and using the data in Table I. We take $L = 33$ and obtain $F_c \approx 0.0066$; this value is indicated on Fig. 5. Also shown is the prediction of Eq. (17) for $\langle \sin^2 \theta^{\text{mid}} \rangle$ as a function of F, for $F > F_c$. These predictions are reasonably consistent with the simulation results. However, it is clear that a value of K^* obtained by inverting this procedure would not be very accurately determined.

IV. DISCUSSION AND CONCLUSIONS

We have calculated the elastic constant K^* as a function of temperature for the Lebwohl-Lasher model using fluctuation expressions and a perturbation method, and have also simulated the Fréedericksz transition for this system, extending the original work of Simpson.[23] Results from the first two methods are consistent with each other, and show that the ratio $K^*/\overline{P}_2^2$ increases as the transition to a disordered phase is approached from below. The Fréedericksz transition occurs at a critical field consistent with the independently measured K^*, but the form of the field-induced response curve and the observation of very slow fluctuations as $F \to F_c$ indicate that this is an inaccurate and ineffective way of determining K^*.

The question remains: which is the most efficient route to an accurate value of K^*? Each of the five sets of fluctuation measurement simulations took 50 h of computer time. The statistics of these measurements were improved by a factor of $\sqrt{2}$ due to the equivalence of the modes $\alpha = 1, 2$. The perturbed system results for the phase points lying inside the linear regime took 16–20 h each. Thus, taking into account the time spent simulating points outside this regime as well as that needed for equilibration and production at the smaller F values, we estimate that about 150 h of computer time were used at each of the temperatures studied. The fluctuation results have substantially better statistics, however, and a major advantage of this method is that fluctuations at a great number of wave vectors are calculated simultaneously. Bearing in mind the importance of establishing the **k** dependence of the results in either case, the equilibrium fluctuation method seems preferable.

The temperature dependence of $K^*/\overline{P}_2^2$ can be compared with theoretical predictions and with experiment. Standard molecular-field theory[1,5] predicts $K_\alpha \propto \overline{P}_2^2$, and for this specific model Priest[22] has calculated $K^*/\overline{P}_2^2 = 3$ for all $T < T_{N\text{-}I}$. This result is in fact only correct as $T \to 0$. While early experimental measurements[8] of $K/\overline{P}_2^2$ found no discernible temperature dependence, subsequent studies[32] detected significant variation with T. In most cases, $K/\overline{P}_2^2$ decreased as T rose, but in a few cases the reverse trend was seen. An alternative approach[33] has been to fit to the more general power law $K_\alpha \propto \overline{P}_2^x$. Again, most fits were found to give $x > 2$ (i.e., a decrease in $K_\alpha/\overline{P}_2^2$ with increasing T, since P_2 shows such a decrease), but those for K_2 yielded $1.74 < x < 2.01$; our results give $x = 1.76$ when analyzed this way.

There are a number of more complicated molecular-field treatments[25,30] which attempt to explain the temperature dependence of $K^*/\overline{P}_2^2$. These theories yield an expansion of the form

$$K = \sum_l \sum_{l' \geq l} c_{ll'} \overline{P}_l \overline{P}_{l'}, \quad l, l' = 2, 4, \ldots \tag{20}$$

where the $c_{ll'}$ are determined by the form of the intermolecular potential. Since the expansion (20) converges rapidly, it is usually truncated after the second term. We have fitted our data for $K^*/\overline{P}_2^2$, $\overline{P}_2$, and $\overline{P}_4$ to this curtailed form to obtain c_{22} and c_{24} "experimentally." Using Priest's exact result for $T = 0$, this one-parameter fit yields $c_{22} = 3.905$, $c_{24} = -0.905$. The corresponding curve, illustrated in Fig. 2, is reasonably consistent with our simulation results. Unfortunately, however, when we apply the methods of Refs. 25 and 30 to this particular model we obtain $c_{24} \equiv 0$ (see Appendix B), so the modified molecular-field theories *cannot* explain the temperature dependence in this case. This failure suggests that the temperature dependence of $K^*/\overline{P}_2^2$ is due to fluctuations completely neglected in these molecular-field theories. It also demonstrates that it is not necessary to invoke strongly anisotropic short-range forces[30] to explain a temperature-dependent $K^*/\overline{P}_2^2$ (although that is not to suggest that such forces are unimportant). However, it does imply that it might be incorrect to interpret experimental Frank-constant data entirely on the basis of molecular-field arguments, no matter how sophisticated the molecular model.

A spin-wave theory, which does take some account of orientational fluctuations has been proposed by Berreman[34] and extended by Faber.[35] In both cases the theory predicts a link between the order parameter $\overline{P}_2$ and the elastic constant K. Berreman's formula is (in our notation)

$$\frac{Ka(1-\overline{P}_2)}{k_B T} = \frac{K^*(1-\overline{P}_2)}{T^*} = C, \tag{21}$$

where a is the lattice spacing and the constant C is evaluated as a sum over cubic reciprocal-lattice points. Faber's derivation takes account of large-amplitude librations, and this leads him to replace the term $(1-\overline{P}_2)$ by $-\ln \overline{P}_2$. Also the constant C is evaluated approximately, by **k**-space integration rather than summation, but this is a minor difference. It turns out, however, that neither theory gives an accurate value for C without modification to correctly account for the amplitudes of the high-k modes in this lattice system. We discuss this in Appendix C. With this modification we obtain $C = 0.7371$.

To compare our results with these expressions we present in Table V the calculated values of $K^*(1-\overline{P}_2)/T^*$ and $K^*(-\ln \overline{P}_2)/T^*$. These are plotted in Fig. 6, and

TABLE V. Tests of spin-wave theory.

T^*	$K^*(1-\overline{P}_2)/T^*$	$-K^*\ln\overline{P}_2/T^*$
0.10	0.722	0.754
0.40	0.682	0.721
0.75	0.613	0.698
0.75[a]	0.617	0.703
0.90	0.573	0.688
1.00	0.519	0.661
1.08	0.412	0.580

[a]Results for the 32 × 32 × 16 system; all others are for 32 × 32 × 32.

they extrapolate smoothly to the spin-wave value at $T^* = 0$. The Faber ratio remains almost constant up to $T^* \approx 0.9$, i.e., $T/T_{N\text{-}I} \approx 0.8$, while the Berreman formula shows marked deviation from the $T^* = 0$ limit at rather lower temperatures.

We can express our results in terms of a **k**-dependent elastic constant defined for our system by

$$K^*(\mathbf{k}) = \frac{9}{4}\left(\frac{\overline{P}_2^2 V T^*}{k^2\left\langle \hat{Q}_{\alpha 3}(\mathbf{k})\hat{Q}_{\alpha 3}(-\mathbf{k})\right\rangle_0}\right), \quad \alpha = 1,2. \tag{22}$$

This is shown in Fig. 7, at several temperatures, for **k** in the (1,1,1) reciprocal-lattice direction. Also shown is the spin-wave ($T^* = 0$) approximation for this quantity, discussed in Appendix C, and curves obtained by scaling the spin wave form to fit the $\mathbf{k} = \mathbf{0}$ value of K at the higher temperatures. This scaled spin-wave prediction fits the data quite well even at high T^*; presumably this is associated with the simple form of the potential for this model, and it is consistent with the accuracy of the Faber and Berreman formulas.

We have commented already on some interesting features of the Fréedericksz transition as simulated for this model. Our main conclusion is that, despite requiring very long runs, our estimate of F_c must be subject to an error of 5–10%. This makes it a very inefficient way of determining K^* computationally. A further caveat is that in any inhomogeneous system finite-size effects will be significant. The original simulations of Simpson[23] employed a 10 × 10 × 10 system. We were able to use a larger system in all dimensions, but particularly in the slab thickness: 16 × 16 × 34. The order parameter $\overline{P}_2(z)$ certainly varies across the simulation box and this variation is most marked close to the fixed boundaries. Thus, any value for the Frank constant obtained by this method will be some sort of average over a range of $\overline{P}_2$. The approximation $\overline{P}_2(z) \simeq$ const becomes less accurate as the slab thickness is decreased. Notwithstanding these reservations, it is interesting to note that the estimates obtained from Simpson's simulations[23,37] of $K^*/\overline{P}_2^2 =$ 3.56, 3.68, and 3.96 at $T^* = 0.90$, 1.00, and 1.08, respectively, are quite close to our own results, reported in Table I.

In conclusion, it seems from the results of our simulations that it is satisfactory to calculate the Frank elastic constants by taking the low-wave-vector limit of the appropriate fluctuation expression. The simple form of the model employed here has allowed us to use a large system to test this procedure, but the results suggest that smaller systems could be employed without jeopardizing the accuracy of the method, provided that attention is paid to wave-vector dependence. It is also possible to

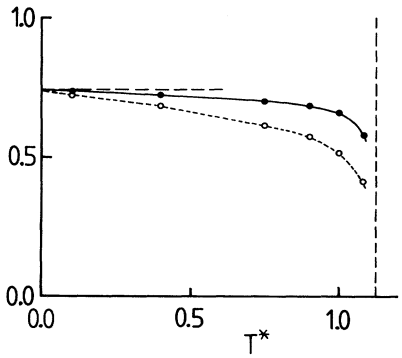

FIG. 6. The ratios $K^*(1-\overline{P}_2)/T^*$ (open circles) and $K^*(-\ln\overline{P}_2)/T^*$ (solid circles) vs T^*. The lines through the data points are to guide the eye. The spin-wave prediction is shown by the horizontal dashed line. The vertical dashed line indicates the nematic-isotropic phase transition temperature $T^*_{N\text{-}I} = 1.1255$.

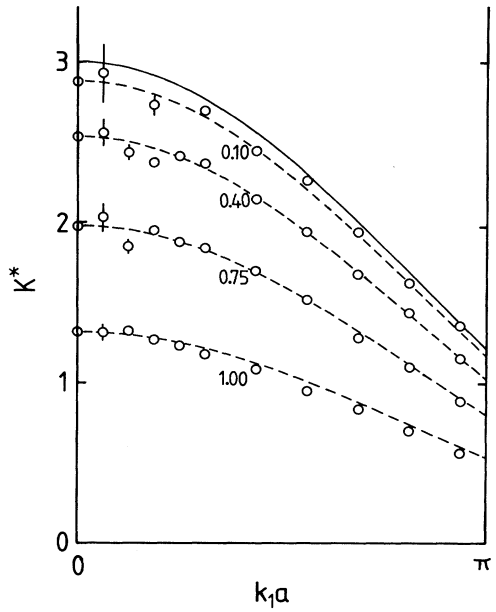

FIG. 7. Wave-vector-dependent elastic constants $K^*(\mathbf{k})$ for $\mathbf{k} = k_1(1,1,1)$. We show the simulation results at $T^* = 0.10$, 0.40, 0.75, and 1.00. The predictions of $T^* = 0$ spin-wave theory, Eq. (C13) (solid line), and the spin-wave form scaled to the zero-k values of K at higher temperatures (dashed lines) are also shown.

calculate the elastic constants by a formally equivalent applied field method, but in view of the limitation to single wave-vector perturbations (or superpositions of a few such perturbations) and the need to check for linearity of response, it is doubtful whether this gives greater efficiency overall. Simulation of the Fréedericksz transition is an interesting and challenging area of research in its own right, but does not constitute a reliable and accurate route to the elastic constants.

Note added in proof. Equation (C13), and the corresponding analysis giving the value of C used in Eq. (21) of the text, have appeared in: T. E. Faber, Proc. R. Soc. London Ser. A **370**, 509 (1980). We are grateful to T. E. Faber for pointing this out.

ACKNOWLEDGMENTS

We acknowledge helpful discussions with R. Evans, M. M. Telo da Gama, and G. R. Luckhurst, who also directed us to the material appearing in P. Simpson's thesis. This work was supported by the United Kingdom Science and Engineering Research Council (SERC), through the provision of an Active Memory Technology DAP 510-8 parallel processor, under the Computational Science Initiative, and through an SERC quota grant to D.J.C.

APPENDIX A: THEORY OF THE FRÉEDERICKSZ TRANSITION

Here we relate the critical field F_c at which the Fréedericksz transition takes place to the elastic constant for our perturbation Hamiltonian, Eq. (15), and discuss the behavior of the system for $F > F_c$. We follow the derivation of Saupe.[1,5,7]

Consider a slab geometry in which molecules are perfectly aligned in a chosen direction **s** at both top and bottom surfaces (perpendicular to the z direction). A uniform bulk field is applied which favors alignment in a direction **f**, perpendicular to **s**. If **s** and **f** are chosen to lie along two of the Cartesian axes then the field will induce a pure twist, bend, or splay deformation, governed by the appropriate elastic constant K_α. In the current model all the elastic constants are equal and it is not necessary to specify any relation between the various axes, other than that **s** and **f** shall be mutually perpendicular.

We may assume that as z varies the director rotates in the **s**-**f** plane, i.e.,

$$\mathbf{n} = \mathbf{s}\cos\theta + \mathbf{f}\sin\theta, \tag{A1}$$

$\theta = \theta(z)$ being the rotation angle. At the surface, $z = 0$, $\theta = 0$. In a semi-infinite system $\theta \to \pi/2$ as $z \to \infty$, but in a slab of thickness L, θ attains its maximum value θ^{mid} at the midpoint $z = L/2$.

The bulk field perturbation term in the Hamiltonian $\mathcal{H} = \mathcal{H}_0 - \Delta\mathcal{H}$ may be written in terms of the orientation tensor density

$$\Delta\mathcal{H} = F\,\mathbf{f}\cdot\hat{\mathbf{Q}}(\mathbf{0})\cdot\mathbf{f} = F\int d\mathbf{r}\;\mathbf{f}\cdot\mathbf{Q}(\mathbf{r})\cdot\mathbf{f}. \tag{A2}$$

Taking the director-based (1,2,3) coordinate system to rotate with **n**, keeping **n** in the 3 direction as usual, and assuming that the orientational distribution is otherwise unperturbed, we may use the diagonal form of $\langle\mathbf{Q}\rangle$ in this representation to evaluate the average energy density as a function of z. We have $\langle Q_{11}\rangle = \langle Q_{22}\rangle = -\frac{1}{2}\overline{P}_2$, $\langle Q_{33}\rangle = \overline{P}_2$, and so $\mathbf{f}\cdot\mathbf{Q}(\mathbf{r})\cdot\mathbf{f} = \overline{P}_2\left(\frac{3}{2}\sin^2\theta - \frac{1}{2}\right)$, $\overline{P}_2$ being the order parameter. Hence the field-induced energy density is

$$\Delta f_{\text{field}} = -F\,\mathbf{f}\cdot\mathbf{Q}(\mathbf{r})\cdot\mathbf{f} = -F\overline{P}_2\left(\tfrac{3}{2}\sin^2\theta - \tfrac{1}{2}\right). \tag{A3}$$

This gives rise to a torque density

$$\tau_{\text{field}} = 3F\overline{P}_2\sin\theta\cos\theta. \tag{A4}$$

The free-energy density due to distortion of the director field is

$$\Delta f_{\text{distortion}} = \tfrac{1}{2}K\left(\frac{d\theta}{dz}\right)^2 \tag{A5}$$

and this gives rise to a torque density

$$\tau_{\text{distortion}} = K\left(\frac{d^2\theta}{dz^2}\right). \tag{A6}$$

The total torque on a volume element of the system must vanish, so

$$K\left(\frac{d^2\theta}{dz^2}\right) + 3F\overline{P}_2\sin\theta\cos\theta = 0. \tag{A7}$$

We may identify the magnetic correlation length ξ by

$$\xi^2 = K/3F\overline{P}_2 \tag{A8}$$

and write

$$\xi^2\left(\frac{d^2\theta}{dz^2}\right) + \sin\theta\cos\theta = 0. \tag{A9}$$

The same equation is obtained in Saupe's derivation, but with $\xi^2 = K/\chi_a H^2$, H being the magnetic field and χ_a the volume anisotropy of the diamagnetic susceptibility. From this point onward the derivation is completely standard.[1] Multiplication by $d\theta/dz$ yields

$$\frac{d}{dz}\left[\xi^2\left(\frac{d\theta}{dz}\right)^2 + \sin^2\theta\right] = 0. \tag{A10}$$

The undistorted solution $\theta \equiv 0$ always satisfies this equation, but above the critical field the distorted solution will be the more stable. Integration gives

$$\xi^2\left(\frac{d\theta}{dz}\right)^2 + \sin^2\theta = \sin^2\theta^{\text{mid}}, \tag{A11}$$

where the constant is determined by the vanishing of $(d\theta/dz)$ at $\theta = \theta^{\text{mid}}$. On taking the square root and separating variables, this gives

$$\frac{L}{2\xi} = \int_0^{\theta^{\text{mid}}} d\theta\,\frac{1}{(\sin^2\theta^{\text{mid}} - \sin^2\theta)^{1/2}}. \tag{A12}$$

This equation is usefully rewritten in terms of a new variable λ defined by $\sin\lambda = \sin\theta/\sin\theta^{\text{mid}}$:

$$\frac{L}{2\xi} = \int_0^{\pi/2} d\lambda \frac{1}{(1-\sin^2\theta^{\rm mid}\sin^2\lambda)^{1/2}}. \quad \text{(A13)}$$

The critical field is determined by setting $\theta^{\rm mid} = 0$, from which $\xi_c = L/\pi$ and

$$F_c = \frac{K\pi^2}{3\overline{P}_2 L^2}. \quad \text{(A14)}$$

This is Eq. (16) of the text.

An alternative route to this equation is to write $\theta(z)$ as a Fourier series

$$\theta(z) = \sum_k \theta_k \sin kz, \quad \text{(A15)}$$

with k an integer multiple of π/L. Then, assuming that $\theta(z)$ is everywhere small enough to write $\sin^2\theta \approx \theta^2$, the free energy per unit area relative to the undistorted state can be expressed

$$\frac{\Delta\mathcal{F}}{A} = \frac{L}{2}\sum_k \theta_k^2(\tfrac{1}{2}Kk^2 - \tfrac{3}{2}F\overline{P}_2). \quad \text{(A16)}$$

The undistorted state will be stable provided this remains positive for distortions of all wavelengths. The lowest-wavelength mode, with $k = \pi/L$, will dictate the point at which distortion becomes energetically favorable; choosing this value and equating the term in parentheses to zero yields Eq. (A14) immediately.

The difference between this result and Saupe's equation [Eq. (13) of the text] arises simply through the different relationship between the field and the correlation length. For the same reason the form of the equation linking $\theta^{\rm mid}$ and the applied field F is slightly different. Direct substitution into Eq. (A13) gives

$$\frac{F}{F_c} = \left(\frac{2}{\pi}\int_0^{\pi/2} d\lambda \frac{1}{(1-\sin^2\theta^{\rm mid}\sin^2\lambda)^{1/2}}\right)^2, \quad \text{(A17)}$$

valid for $F > F_c$, and this is Eq. (17) of the text. Finally we note that, for our lattice system, spatial integrals should be replaced by sums in the above derivation, and the key differential equation, Eq. (A9), then becomes a difference equation. For a system of the size treated here we have verified that this discretization makes a negligible difference to the final results.

APPENDIX B: ELASTIC CONSTANT EXPANSION

Here we apply the methods of Refs. 25 and 30 to the potential of Eq. (3), and show that, within this molecular-field approximation, the expansion coefficients $c_{ll'}$ of Eq. (20) vanish, except when $l = l' = 2$. To this end we consider a distortion of the director field $\mathbf{n}(\mathbf{r})$. The orientation $\mathbf{e}$ of a molecule is distributed about the director $\mathbf{n}$ according to the function $\mathcal{P}(\mathbf{n}\cdot\mathbf{e})$. The distribution function for a neighboring molecule will be assumed to be $\mathcal{P}(\mathbf{n}'\cdot\mathbf{e}')$, where the director $\mathbf{n}'$ is slightly rotated from $\mathbf{n}$; this is the only effect taken into account. For the potential of Eq. (3), the average interaction energy between these two molecules is

$$\overline{\mathcal{H}(\mathbf{n},\mathbf{n}')} = -\varepsilon\int d\mathbf{e}\int d\mathbf{e}'\mathcal{P}(\mathbf{n}\cdot\mathbf{e})\mathcal{P}(\mathbf{n}'\cdot\mathbf{e}')P_2(\mathbf{e}\cdot\mathbf{e}'), \quad \text{(B1)}$$

where $\int d\mathbf{e}\cdots$ stands for integration over the polar angles $\int d\phi \int \sin\theta\, d\theta \cdots$. Assuming that the distribution functions are undistorted by the director variation, they may be expanded in Legendre polynomials:

$$\mathcal{P}(\mathbf{n}\cdot\mathbf{e}) = \sum_l \left(\frac{2l+1}{4\pi}\right)\overline{P}_l P_l(\mathbf{n}\cdot\mathbf{e}) \quad \text{(B2)}$$

to give

$$\overline{\mathcal{H}(\mathbf{n},\mathbf{n}')} = -\varepsilon\int d\mathbf{e}\int d\mathbf{e}'\sum_l\sum_{l'}\left(\frac{2l+1}{4\pi}\right)\left(\frac{2l'+1}{4\pi}\right)\overline{P}_l\,\overline{P}'_l\,P_l(\mathbf{n}\cdot\mathbf{e})\,P_{l'}(\mathbf{n}'\cdot\mathbf{e}')\,P_2(\mathbf{e}\cdot\mathbf{e}'). \quad \text{(B3)}$$

For a more general interaction potential the $P_2(\mathbf{e}\cdot\mathbf{e}')$ function would be replaced by a sum of Legendre polynomials, and this would give rise to the expansion of the form $\sum_l\sum_{l'} c_{ll'}\overline{P}_l\overline{P}_{l'}$ seen in Eq. (20). In the current case, however, it is easy to show that only one term survives. Each Legendre polynomial may be expanded in spherical harmonics C_{lm} in the following way:

$$P_l(\mathbf{n}\cdot\mathbf{e}) = \sum_{m=-l}^{l} C_{lm}(\mathbf{n})C^*_{lm}(\mathbf{e}). \quad \text{(B4)}$$

The orthogonality relation

$$\int d\mathbf{e}\, C_{lm}(\mathbf{e})C_{l'm'}(\mathbf{e}) = \delta_{ll'}\delta_{mm'}\left(\frac{4\pi}{2l+1}\right) \quad \text{(B5)}$$

allows the angular integrations to be performed easily, yielding

$$\overline{\mathcal{H}(\mathbf{n},\mathbf{n}')} = -\varepsilon\overline{P}_2^2 P_2(\mathbf{n}\cdot\mathbf{n}'). \quad \text{(B6)}$$

Consequently the change in energy due to the director variation is

$$\overline{\Delta\mathcal{H}(\mathbf{n},\mathbf{n}')} = -\varepsilon\overline{P}_2^2(P_2(\mathbf{n}\cdot\mathbf{n}') - 1) = \frac{3\varepsilon}{2}\overline{P}_2^2\sin^2\theta, \quad \text{(B7)}$$

where θ is the angle between $\mathbf{n}$ and $\mathbf{n}'$. Only the $l = l' = 2$ terms in the Legendre polynomial expansions have survived the angular averaging.

This equation can be used to calculate the elastic constants by taking the variation in $\mathbf{n}$ to be induced by a splay, twist, or bend deformation of chosen wave number k. The free-energy density at a given lattice site will be given by a sum of contributions of the form of Eq. (B7) from each of the neighboring sites, divided by 2 to avoid double counting. Entropic contributions are assumed to be negligible by comparison at low k. Selecting the wave vector $\mathbf{k}$ to lie along one of the lattice axes eliminates contributions from all but two neighbors; for these two the angle θ is equal to ka, a being the lattice spacing. The result is that the change in free-energy density due to director variation is given by

$$\Delta f = \frac{3\varepsilon}{2a^3}\overline{P}_2^2 \sin^2 ka, \tag{B8}$$

which is proportional to k^2 at low k. From this we can identify the elastic constant $K = 3\varepsilon\overline{P}_2^2/a$, or in reduced units $K^*/\overline{P}_2^2 = 3$, as obtained originally by Priest.[22]

Thus, despite the reasonable fit of the expansion of Eq. (20) to our simulation results, we see that the molecular-field arguments on which it is based yield $c_{ll'} \propto \delta_{l2}\delta_{l'2}$ for the Lebwohl-Lasher model. Equation (B3) shows the origins of this expansion, and makes it clear that higher terms in the expansion are directly related to higher-order terms in the interaction potential.

APPENDIX C: SPIN-WAVE THEORY

In this appendix we summarize the spin-wave theory for the order parameter in the Lebwohl-Lasher model. We follow the general arguments of Berreman[34] and Faber,[35] but our main aim is to highlight the need to deal correctly with the high-k modes. We write the Hamiltonian, Eq. (3), in the form

$$\mathcal{H}_0 = -\tfrac{1}{2}\varepsilon\sum_{\mathbf{r}}\sum_{\mathbf{a}}\{\tfrac{3}{2}[\mathbf{e}(\mathbf{r})\cdot\mathbf{e}(\mathbf{r}+\mathbf{a})]^2 - \tfrac{1}{2}\}. \tag{C1}$$

Here $\mathbf{e}(\mathbf{r})$ is the unit vector along the axis of each molecule situated at a position $\mathbf{r}$ on the cubic lattice. $\mathbf{a}$ is one of the six nearest-neighbor lattice vectors, and the factor $\frac{1}{2}$ avoids double counting. Setting $\mathbf{e} = (e_1, e_2, e_3)$ and taking the director along the 3 axis as usual, small orientational fluctuations are described in terms of the components e_1 and e_2. In the usual development $\mathbf{e}(\mathbf{r}+\mathbf{a})$ is expanded in a Taylor series to second order about $\mathbf{e}(\mathbf{r})$. Taking the continuum limit

$$\sum_{\mathbf{r}} \to \frac{1}{a^3}\int d\mathbf{r}$$

and performing an integration by parts yields the usual squared-gradient spin-wave Hamiltonian, which is equivalent to the phenomenological free-energy equation, Eq. (2) of the text. Whether or not this continuum approximation is made, however, the Fourier-series expansions

$$e_\alpha(\mathbf{r}) = \frac{1}{V}\sum_{\mathbf{k}(\neq\mathbf{0})} \hat{e}_\alpha(\mathbf{k})\exp(-i\mathbf{k}\cdot\mathbf{r}), \quad \alpha = 1,2 \tag{C2}$$

allow the Hamiltonian to be written in the form

$$\mathcal{H}_0 = -3N\varepsilon + \frac{1}{2}\left(\frac{3\varepsilon}{a}\right)\frac{1}{V}\sum_{\mathbf{k}} k^2[|\hat{e}_1(\mathbf{k})|^2 + |\hat{e}_2(\mathbf{k})|^2], \tag{C3}$$

where $V = Na^3$ is the volume of the sample. We can immediately identify $K = 3\varepsilon/a$ and use equipartition to deduce

$$\overline{|\hat{e}_1(\mathbf{k})|^2} = \overline{|\hat{e}_2(\mathbf{k})|^2} = \frac{Vk_BT}{Kk^2}. \tag{C4}$$

This is equivalent to Eq. (6), used to determine the Frank constant at all temperatures.

The link with the order parameter is made through Parseval's theorem, which gives us

$$\begin{aligned}\overline{|e_1(\mathbf{r})|^2} &= \frac{1}{V^2}\sum_{\mathbf{k}}\overline{|\hat{e}_1(\mathbf{k})|^2} \\ &= \frac{k_BT}{KV}\sum_{\mathbf{k}}\frac{1}{k^2} = \frac{k_BT}{Ka}\left\langle\frac{1}{k^2a^2}\right\rangle_{BZ},\end{aligned} \tag{C5}$$

where we introduce the Brillouin-zone average $\langle\cdots\rangle_{BZ} \equiv N^{-1}\sum_{\mathbf{k}}(\cdots)$, the sum being over the N points (except the origin) in the first Brillouin zone. The same equation applies for $\overline{|e_2(\mathbf{r})|^2}$. The order parameter is then written

$$\begin{aligned}\overline{P_2} &= \tfrac{3}{2}\overline{e_3(\mathbf{r})^2} - \tfrac{1}{2} = 1 - \tfrac{3}{2}[\overline{e_1(\mathbf{r})^2} + \overline{e_2(\mathbf{r})^2}] \\ &= 1 - \frac{3k_BT}{Ka}\left\langle\frac{1}{k^2a^2}\right\rangle_{BZ}.\end{aligned} \tag{C6}$$

Thus we arrive at Berreman's formula, Eq. (21); we obtain $C = 0.5616$ for a cubic system, $N = 32 \times 32 \times 32$. This underestimates the observed low-temperature variation of $\overline{P}_2$ by 30%.

The error arises because of the restriction to low k implicit in the original Taylor-series expansions of $e_\alpha(\mathbf{r})$, and the resulting k^2 (squared-gradient) form of the Hamiltonian. A formula correct at all k is obtained by setting

$$e_\alpha(\mathbf{r}+\mathbf{a}) = \frac{1}{V}\sum_{\mathbf{k}\neq\mathbf{0}}\exp(-i\mathbf{k}\cdot\mathbf{a})\hat{e}_\alpha(\mathbf{k})\exp(-i\mathbf{k}\cdot\mathbf{r}), \quad \alpha = 1,2. \tag{C7}$$

The nearest-neighbor interaction term may be expanded, assuming small relative angular displacements,

$$\begin{aligned}&P_2(\mathbf{e}(\mathbf{r})\cdot\mathbf{e}(\mathbf{r}+\mathbf{a})) \\ &\approx 1 - \tfrac{3}{2}\{\,[e_1(\mathbf{r}) - e_1(\mathbf{r}+\mathbf{a})]^2 \\ &\qquad + [e_2(\mathbf{r}) - e_2(\mathbf{r}+\mathbf{a})]^2\},\end{aligned} \tag{C8}$$

and the orientation-dependent terms, when summed over $\mathbf{r}$ for fixed $\mathbf{a}$ become

$$\sum_{\mathbf{r}}[e_\alpha(\mathbf{r}) - e_\alpha(\mathbf{r}+\mathbf{a})]^2 = \frac{1}{V^2}\sum_{\mathbf{k}}[1-\exp(i\mathbf{k}\cdot\mathbf{a})][1-\exp(-i\mathbf{k}\cdot\mathbf{a})]|e_\alpha(\mathbf{k})|^2 = \frac{1}{V^2}\sum_{\mathbf{k}}2[1-\cos(\mathbf{k}\cdot\mathbf{a})]|e_\alpha(\mathbf{k})|^2. \quad \text{(C9)}$$

This $2[1-\cos(\mathbf{k}\cdot\mathbf{a})]$ form, familiar from standard spin-wave analysis of the Heisenberg model[36] tends to the k^2a^2 limit at low k. However, these low-k modes do not completely dominate the Brillouin-zone average (because of the effective k^2 weighting in the sum or integral over reciprocal space), so it is important to retain this full form. Performing a sum over all six nearest-neighbor vectors $\mathbf{a}$ gives the new equipartition result for orientational fluctuations

$$\overline{|\hat{e}_\alpha(\mathbf{k})|^2} = \frac{Vk_BT}{K}\left(\frac{a^2}{6-2\cos k_xa-2\cos k_ya-2\cos k_za}\right) \quad \text{(C10)}$$

where $\mathbf{k}=(k_x,k_y,k_z)$. [Note that the lattice-based (x,y,z) coordinate system can be taken to be quite independent of the director-based $(1,2,3)$ coordinate system here.] The final result, which is to be compared with Eq. (C6), is

$$\overline{P_2} = 1 - \frac{3k_BT}{Ka}\left\langle\frac{1}{6-2\cos k_xa-2\cos k_ya-2\cos k_za}\right\rangle_{BZ}. \quad \text{(C11)}$$

Now the Brillouin-zone average gives us Eq. (21) of the text, with $C = 0.7371$ for our cubic $N = 32\times32\times32$ system.

We can express these results in terms of a $\mathbf{k}$-dependent elastic constant, defined by

$$K(\mathbf{k}) \equiv \frac{Vk_BT}{k^2\overline{|\hat{e}_\alpha(\mathbf{k})|^2}}. \quad \text{(C12)}$$

The spin-wave prediction gives us

$$K(\mathbf{k}) = K\left(\frac{6-2\cos k_xa-2\cos k_ya-2\cos k_za}{k^2a^2}\right). \quad \text{(C13)}$$

At low k we see $K(\mathbf{k}\to\mathbf{0}) = K$ but $K(\mathbf{k})$ decreases towards the Brillouin zone boundary. Equation (C13) is expected to hold at low temperature, with $K = 3\varepsilon/a$, but it may also be used to fit the observed $K(\mathbf{k})$ at higher temperatures, with K chosen to equal the observed $\mathbf{k}=\mathbf{0}$ value. This is illustrated in Fig. 7 of the text.

*Corresponding author.

[1] P. G. de Gennes, *The Physics of Liquid Crystals* (Clarendon, Oxford, 1974).
[2] D. Forster, *Hydrodynamic Fluctuations, Broken Symmetry and Correlation Functions*, Vol. 47 of *Frontiers in Physics*, (Benjamin, Reading, 1975).
[3] F. C. Frank, Discuss. Faraday Soc. **25**, 19 (1958).
[4] Note, however, that the description of flow requires a number of other phenomenological constants. See, e.g., F. Leslie, in *Theory and Applications of Liquid Crystals*, edited by J. L. Ericksen and D. Kinderlehrer (Springer-Verlag, New York, 1987), p. 235
[5] S. Chandrasekhar, *Liquid Crystals* (Cambridge University Press, Cambridge, England, 1977).
[6] V. Fréedericksz and V. Zolina, Trans. Faraday Soc. **29**, 919 (1933).
[7] A. Saupe, Z. Naturforsch. A **15**, 815 (1960) (in German). A comprehensive alternative in English is H. Gruler, T. Scheffer, and G. Meier, *ibid.* A **27**, 966 (1972).
[8] I. Haller, J. Chem. Phys. **57**, 1400 (1972).
[9] H. Gruler and G. Meier, Mol. Cryst. Liq. Cryst. **16**, 299 (1972).
[10] P. R. Gerber and M. Schadt, Z. Naturforsch. A **35**, 1036 (1980).
[11] S. Shtrikman, E. P. Wohlfarth, and Y. Wand, Phys. Lett. A **37**, 369 (1971).
[12] J. L. Martinand and G. Durand, Solid State Commun. **10**, 815 (1972); D. A. Dunmur and K. Szumlin, Liquid Crystals **6**, 449 (1989).
[13] S. Faetti and V. Palleschi, Liquid Crystals **2**, 261 (1987).
[14] P. A. Lebwohl and G. Lasher, Phys. Rev. A **6**, 426 (1972); **7**, 2222(E) (1973).
[15] W. Maier and A. Saupe Z. Naturforsch. A **13**, 564 (1958); **14**, 882 (1959); **15**, 287 (1960).
[16] C. Zannoni, in *Molecular Physics of Liquid Crystals*, edited by G. R. Luckhurst and G. W. Gray (Academic, New York, 1979), p. 191.
[17] G. R. Luckhurst and P. Simpson, Mol. Phys. **47**, 251 (1982).
[18] U. Fabbri and C. Zannoni, Mol. Phys. **58**, 763 (1986).
[19] G. R. Luckhurst, T. J. Sluckin, and H. B. Zewdie, Mol. Phys. **59**, 657 (1986).
[20] M. P. Allen, Mol. Sim. **4**, 61 (1989).
[21] M. M. Telo da Gama, P. Tarazona, M. P. Allen, and R.

Evans, Mol. Phys. **71**, 801 (1990).
[22]R. G. Priest, Mol. Cryst. Liq. Cryst. **17**, 129 (1972).
[23]P. Simpson, Ph.D. thesis, University of Southampton, 1980.
[24]L. Onsager, Ann. N. Y. Acad. Sci. **51**, 627 (1949).
[25]R. G. Priest, Phys. Rev. A **7**, 720 (1973).
[26]J. P. Straley, Phys. Rev. A **8**, 2181 (1973); A. Poniewierski and J. Stecki, Mol. Phys. **38**, 1931 (1979); E. Govers and G. Vertogen, Liquid Crystals **5**, 323 (1989); Y. Singh and K. Singh, Phys. Rev. A **33**, 3481 (1986).
[27]M. P. Allen and D. Frenkel, Phys. Rev. A **37**, 1813 (1988). Note that the results presented in this paper are in error by a factor $\frac{9}{4}$; see the recently printed Erratum, Phys. Rev. A **42**, 3641 (1990).
[28]M. P. Allen, D. Frenkel, and J. Talbot, Comput. Phys. Rep. **9**, 301 (1989).
[29]J. Nehring and A. Saupe, J. Chem. Phys. **56**, 5527 (1972); E. Govers and G. Vertogen, Liquid Crystals **2**, 31 (1987).
[30]W. M. Gelbart and A. Ben-Shaul, J. Chem. Phys. **77**, 916 (1982).
[31]R. Eppenga and D. Frenkel, Mol. Phys. **52**, 1303 (1984).
[32]H. Gruler, Z. Naturforsch. A **30**, 230 (1975); W. H. de Jeu and W. A. P. Claassen, J. Chem. Phys. **67**, 3705 (1977); F. Leenhoots and A. J. Dekker, J. Chem. Phys. **74**, 1956 (1981).
[33]P. P. Karat and N. V. Mahudusana, Mol. Cryst. Liq. Cryst. **40**, 239 (1977).
[34]D. W. Berreman, J. Chem. Phys. **62**, 776 (1975).
[35]T. E. Faber, Proc. R. Soc. London Ser. A **353**, 247 (1977).
[36]R. P. Feynman, *The Feynman Lectures in Physics III* (Addison-Wesley, Reading, MA, 1964).
[37]Note that an error of a factor of $\frac{3}{2}$ was made in relating the critical field to the elastic constant in Ref. 23. In quoting Simpson's results we have included this correction.